Geomorphology 138 (2012) 295–305

Contents lists available at SciVerse ScienceDirect

Geomorphology

journal homepage: www.elsevier.com/locate/geomorph

Novel particle method for modelling the episodic collapse of soft coastal bluffs

Johan Vandamme [a,*], Qingping Zou [b], Ed Ellis [c,1]

[a] Centre for Coastal Dynamics and Engineering, School of Marine Science and Engineering, University of Plymouth, UK
[b] Department of Civil and Environmental Engineering, University of Maine, Orono, ME 04469, USA
[c] School of Marine Science and Engineering, University of Plymouth, UK

ARTICLE INFO

Article history:
Received 15 July 2011
Received in revised form 7 September 2011
Accepted 8 September 2011
Available online 16 September 2011

Keywords:
Coastal bluffs
Episodic failure
Model
Collapse
Stability

ABSTRACT

This paper presents a new, novel, particle-based Bluff Morphology Model (BMM), and with it investigates the stability, collapse, and equilibrium position of soft coastal bluffs (cliffs). This model combines a multiple wedge displacement method with an adapted Weakly Compressible Smoothed Particle Hydrodynamics (WCSPH) method. At first, the wedge method is applied to compute the stability of the bluff. Once the critical failure mechanism of the bluff slope has been identified, and if the factor of safety for the mechanism is less than 1, the adapted WCSPH method is used to predict the failure movement and residual shape of the slope. The model is validated against benchmark test cases of bluff stability for purely frictional, purely cohesive, and mixed strength bluff materials including 2D static water tables. The model predictions give a good correlation with the expected values, with medium resolution models producing errors of typically less than 2.0%. In addition, the prediction of lateral movement of a surveyed cliff and the dynamic collapse of a vertical bluff are computed, and compare well with published literature.

1. Introduction

The development of climate change predictions, combined with the increasing risk and value of coastal and marine assets, has prompted a surge in interest in the modelling and predictions of coastal, shoreline and bluff movements. It is imperative that the mechanisms of coastal bluff collapse are fully understood in order to predict the location of a slope failure and improve the accuracy of quantified asset risk and implement appropriate stabilisation measures. This knowledge, however, requires a full assessment of factors affecting coastal bluff stability and collapse over short timescales.

Much of the previous research in the field of coastal landsliding has focused on understanding why landslides form through a retrospective analysis, either by considering the ground profile following a slip or by considering mechanisms and processes that cause mass failures, allowing for a empirical models (Walkden and Hall, 2005; Trenhaile, 2009), or by gaining a data set that allows a probabilistic extrapolation (Lee et al., 2001; Furlan, 2008). Although coastal landsliding typically consists of large episodic collapses, there has been a considerable amount of research that considers spatially and temporally diluted monitoring systems, which result in significant smoothing of the dramatic collapse episodes themselves. Quinn et al. (2010) considers this to be directly contributing to a poor understanding of coastal slope processes.

As a result of this, and the spatial variability of the coastlines studied, there is significant debate about the key factors that control failure events and occurrences associated with bluff failure. Some individual mechanisms are well documented, for example Hutchinson(1970) and Dixon and Bromhead(2002), yet there is little in the way of a numerical model with which coastal slope failures can be back-analysed and the failure mechanism best identified. The authors believe that this is primarily due to the complexity of the issue at hand, where any such model must consider a wide range of factors in order to attempt to replicate a failure event with any accuracy. These factors include the geological layering (Bromhead and Ibsen, 2004), rainfall and pore water pressures (Caine, 1980; Iverson, 2000), particle orientation and cementation (Martins et al., 2005) and toe erosion (Walkden and Dickson, 2008).

Research on the modelling of short term coastal cliff and bluff erosion is still relatively unexplored. Although there are several models of beach profile change, most of these are closed loop models which, under constant boundary conditions, tend towards an equilibrium beach profile. SBEACH (Larson and Kraus, 1989; Larson et al., 1989) is a two dimensional cross-shore model which takes the significant destructive force to be that of the dissipation of wave energy per unit volume of water. It incorporates wave run-up and wave set-up and outputs an accurate, although marginally under-predicted (Zheng and Dean, 1997) dune profile. SBEACH is similar in both method and results to EDUNE (Kriebel and Dean, 1985; Kriebel, 1986). EDUNE models a constant wave run-up but neglects set-up and variable sediment properties.

Other equilibrium profile methods include the Coastal Construction Control Line (CCCL) (Chiu and Dean, 1984; Chiu and Dean, 1986). This

* Corresponding author. Fax: +44 1752 232638.
E-mail addresses: johan.vandamme@plymouth.ac.uk (J. Vandamme), qingping.zou@maine.edu (Q. Zou), edward.ellis@plymouth.ac.uk (E. Ellis).
[1] Fax: +44 1752 586101.

0169-555X/$ – see front matter © 2011 Elsevier B.V. All rights reserved.
doi:10.1016/j.geomorph.2011.09.013

method models a uniform sediment profile, and has a tendency to over-predict results (Zheng and Dean, 1997), and has not been subsequently developed significantly in research literature.

Another popular model is XBEACH (Roelvink et al., 2009). This is a 2D depth-averaged model, which considers the height of the surface to be a scalar parameter, that is designed to model nearshore and dune response during storm events. It is a grid-based model that solves momentum balance and mass transfer on a staggered grid, such that mass balance is solved in cell centres, and momentum balance is solved at cell interfaces. Shallow water momentum equations are solved after Walstra et al. (2000). XBEACH has been shown to have a high sensitivity to storm surge inputs, and a general overestimation of erosion. This could be due, in part, to the avalanching algorithm used to predict dune collapse (McCall, 2008), that is, the algorithm of the model calculates that the dune will collapse when the slope angle is greater than the angle of repose of the dune material but the dune remains constant if the slope angle is less than this.

Applying these types of medium term beach equilibrium models directly to collapse of coastal bluffs and dunes, however, can be problematic. Over a sufficiently long time, all beach profiles will conform to the equilibrium position, but the episodic nature of bluff and cliff erosion is such that the discrete, sudden events are not well captured by transitions among different equilibrium positions (Quinn et al., 2010). The slope stability element is a critical factor in the accuracy of the short term predictions of these models.

When considering the slope stability, XBeach, along with many other nearshore models, uses an avalanching algorithm to define the maximum dune slope, and only considers wave and marine erosion to be the cause of bluff collapse, ignoring the geotechnical, hydrological and geological parameters that would influence the type and size of slip. Slope stability programmes, from a geotechnical field, consider rotational, as well as translational slip failures. Considering all possible types of failure is necessary to ensure that the prediction is as accurate as possible.

The majority of slope stability models use the Swedish (Fellenius) method of slices, or a derivative of this method (Donald and Chen, 1997) to examine the stability of the slope in question. Error margins of this method typically range from 5 to 20% (Craig, 1974) depending on the bluff conditions. This method consistently over-predicts the disturbing force, thus producing a conservative estimate of slope stability. Non-circular failure slopes are conventionally analysed using a multiple wedge method (Donald and Chen, 1999; McCombie, 2009).

A common slope stability software package is SLOPE/W (Krahn, 2004) which analyses the stability of a user-defined slope section with varying earth materials and engineering reinforcements, and under dynamic/seismic loading. Slope/W has a variety of slope analysis methods built in, including the Fellenius method, and derivatives of it, but can also use a Finite Element Method inside a limit equilibrium framework. This affords it a more accurate stress distribution than through the alternative circular arc analyses (Krahn, 2004).

None of these existing models can fully resolve the location, type and equilibrium position of a slope collapse. This paper presents a novel approach, using a particle method, for stability analysis and collapse predictions of a coastal bluff. Using controlled parameters, this method provides detailed slope stability analysis based on a multiple wedge method so that deep-seated rotational failures are considered. This method also incorporates shallow translational "avalanching" failures. In addition to this, once identified, this model allows for the failure mechanism and collapse to be simulated in order to predict the final profile shape of the bluff in question. This is a useful addition to coastal bluff research since a generic slope model which predicts both stability and collapse in a mesh-free, non-distorting method has not yet been published. The applications of this model run beyond back-analysis, and this model could be used to design temporary or permanent works designed to maintain the stability of the bluff, as well as to further understand the nature and development of slip surfaces.

2. Bluff Morphology Model

The model presented in this paper is a particle-based bluff morphology model, which can be used in hybrid with any 2D beach erosion model or data to predict bluff collapse without using an avalanching method.

This model is designed to consider the stability and movement of bluffs made of weak earth materials, which can be adequately modelled as a series of continuous materials where spatial variability such as joints or bedding planes are negligible. This allows it to be applied to both weak coastal bluffs and dunes. When considering a coastal bluff of complex geology, multiple different materials can be modelled by assigning the relevant properties and parameters to the corresponding numerical particles.

The model set-up represents areas of bluff material as computational particles, which are initially tessellated in a hexagonal pattern, and allows for each particle to be assigned specific scalar parameters including mass, pore water pressure, and bluff material type. The bluff material type of the particle indicates both the cohesion and maximum angle of shearing resistance (Φ'). These are both mobilised over a displacement stepping within the model such that peak cohesion and peak Φ' are mobilised at the same displacement, creating a mobilised cohesion (c'_{mob}) and a mobilised angle of shearing resistance (Φ'_{mob}), which are calculated using a user-specified relationship between Φ'_{mob} and displacement. An example of the model visualisation of this relationship is shown in Fig. 1.

In this method, each particle can have a unique set of properties to represent the bluff material. However, this limits the accuracy of representing bluff materials numerically through two ways. First, if the material is highly spatially variable, the accuracy will be limited by the accuracy of the sampling used to investigate the bluff itself. Second, a cliff or bluff material that has significant spatial strength variability, for example a rock with bedding planes and joints, would be too complex to model as the joints and bedding planes can only be modelled through a line of numerical particles, which in turn presents a resolution-based problem. Thus, this study considers homogeneous bluffs to test the accuracy of the model.

The particle model is an advantageous method for predicting sudden collapse of a coastal bluff. With no mesh regeneration or straining under large relative distortion, the model allows for a fully Lagrangian model which can track the history of each particle, ensuring, for

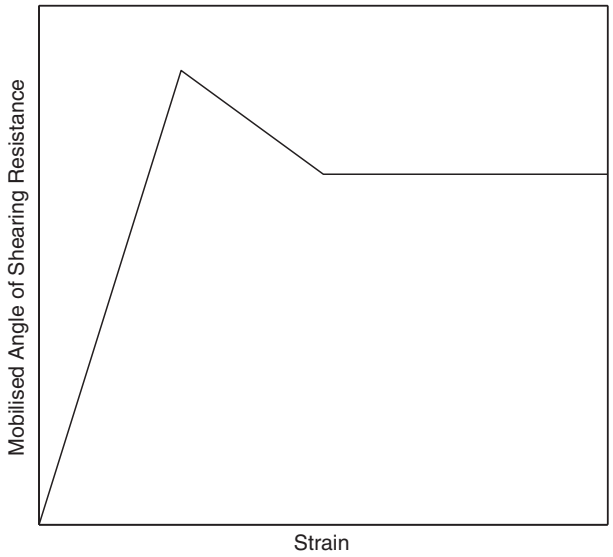

Fig. 1. Assumed relationship between mobilised angle of shearing resistance (Φ'_{mob}) and strain along the assumed failure surface.

example, that bluff material particles on a failure surface will remain as material of a residual strength.

The model has been developed with intent to predict collapse under erosion events. As a result, the particle method can move or remove particles to ensure the bluff profile in the programme correlates well to the profile data. These data can be supplied by any experimental or numerical modelling method. Initial work has been done using a Weakly Compressible Smoothed Particle Hydrodynamics model (Zou, 2007; Vandamme et al., 2009), although the runtimes of the WCSPH model limit the usefulness of this particular partnership.

2.1. Stability analysis

When modelling the stability of the bluff, it was decided to use a wedge analysis as opposed to a traditional circular arc analysis, as this allows a more exhaustive search through the potential slip planes. Using the method presented by McCombie (2009) the model can search throughout the bluff and calculate the mobilised angle of shearing resistance. This subsequently allows accurate predictions of collapse and offers a comprehensive insight into the sub-surface material.

For ease of comprehension, the method of cycling through the calculated failure surfaces is conceptualised in Fig. 2. Initially, the method assumes an entry point of an arbitrary failure surface on the soil surface, and then an exit point above this. Many potential slips that fit these two points are then analysed, from linear to a near-circular analysis where the back of the potential failure surface is vertical (steps 3 and 4 in Fig. 2). If the slip surface daylights (as shown on A in Fig. 2), then the entry point is moved to the appropriate place. The exit point is then stepped across the domain repeating this loop, and then the entry point is moved and the loop begins again. The resolution of calculating the stability planes is determined by the model user, and the potential slip surfaces are cycled through at a rate of approximately 3000 per minute on a standard desktop CPU with a domain of 70,000 particles, and thus it allows the model to compute a wide ranging stability analysis.

Once the failure surface is defined, it is discretized into a number of wedges. These can be arbitrary in location along the plane, however wedge boundaries must coincide with any failure surface vertices in order to ensure compatible displacement along the boundary, such that each wedge displaces linearly. In order to achieve this, the failure surface is constructed with straight lines between the wedge boundaries, as shown by Fig. 3. The number of wedges used is a user-defined variable, and sensitivity analysis for this is discussed for example with Figs. 4 and 6.

Fig. 3 shows an arbitrary failure surface as selected by the model. The wedge boundaries are angled such that they bisect the internal angle of the failure surface equally, due to assuming that any dilation can be neglected (McCombie, 2009). However, this can cause wedge boundaries to intersect, creating a potential source of significant error. When the boundaries do intersect, the wedge boundaries are rotated equally to ensure no overlap within the bluff, however this reduces the accuracy of the force mobilisation on the interwedge boundaries and can subsequently reduce accuracy. Having defined the wedge boundaries, the weight of the wedges and the material properties along each vertex are found and computed.

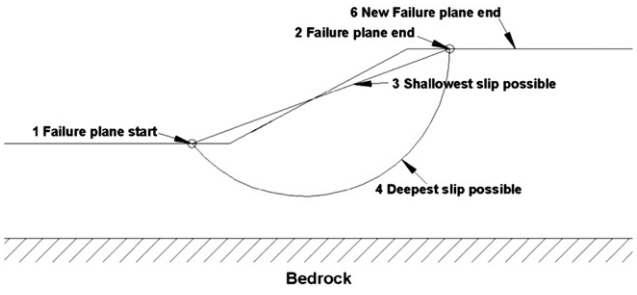

Fig. 2. Conceptualised cycle of mechanism to find failure surfaces.

Beginning with the uppermost wedge, the forces acting on each wedge are resolved in the horizontal and vertical direction, and solved to find the normal forces acting on the wedge from each boundary, i.e. the normal forces (N'). The interwedge boundary force is equal and opposite and subsequently each wedge can be resolved until the final wedge, where a horizontal force that maintains equilibrium is applied and calculated.

Normal forces on the wedges (N) are calculated iteratively over all the wedges, with the force on the interwedge boundaries being reflected, such that:

$$N_{i,1} = N_{i-1,3}\,. \tag{1}$$

The effective force (N') is defined as follows, where N is the normal force, and U the integrated pore water pressure (u) over the wedge boundary:

$$N'_{i,1} = N_{i,1} - U_{i,1}. \tag{2}$$

The shear force on the wedge boundaries, T is the combination of the cohesive force (C') and the product of the angle of shearing resistance of the soil (Φ') computed using the material profile and current displacement, and the effective force (N') from the previous displacement step, such that:

$$T_{i,2} = \left\{C'_{i,2} + \left(N'_{i,2}\right)\tan\left(\Phi'_{i,2}\right)\right\}. \tag{3}$$

Due to the displacement stepping method, the value of T_i will vary with the displacement, and as a result of this, for any given displacement, the mobilised values of c' and Φ' will be referred to as c'_{mob} and Φ'_{mob} respectively.

Starting with the uppermost wedge, the normal forces are found through resolving the forces on the subsequent wedges:

$$\begin{aligned} N'_{i,2} = \frac{1}{\cos(\alpha_i) + \sin(\alpha_i)*\tan(\beta_{i+1})}\Big\{ & W_i - T_{i,1}\left(\sin(\beta_i)*\tan(\beta_{i+1}) + \cos(\beta_i)\right) \\ & + N_{i,1}\left(\sin(\beta_i) - \cos(\beta_i)*\tan(\beta_{i+1})\right) - T_{i,2}\left(\sin(\alpha_i) - \cos(\alpha_i)*\tan(\beta_{i+1})\right) \\ & + T_{i,3}\left(\cos(\beta_{i+1}) + \sin(\beta_{i+1})*\tan(\beta_{i+1})\right)\Big\} - U_{i,2} \end{aligned} \tag{4}$$

$$N'_{i,3} = \frac{1}{\cos(\beta_{i+1})}\left\{T_{i,1}\sin(\beta_i) + N_{i,1}\cos(\beta_i) + N_{i,2}\sin(\alpha_i) - T_{i,2}\cos(\alpha_i) - T_{i,3}\sin(\beta_{i+1})\right\} - U_{i,3} \tag{5}$$

where W_i is the weight of the wedge. When the normal forces acting on the last wedge are known, the last wedge can be resolved in both directions. As this wedge has no value for $N_{i,3}$, a balancing force F_{out} is introduced to keep the mechanism in equilibrium. This horizontal "out of balance" force (F_{out}) can be described as a sum of the wedge forces, as shown in Eq. (1) where the subscript i notates the final wedge.

$$F_{out} = T_{i,1}\sin(\beta_i) + N_{i,1}\cos(\beta_i) + N_{i,2}\sin(\alpha_i) - T_{i,2}\cos(\alpha_i). \tag{6}$$

If this force is positive, the slip mechanism is unstable with the computed shear forces, and the displacement is increased across the slip boundary, and the new values of c'_{mob} and Φ'_{mob} are predicted using a new stability, and the new values of T, which are computed using the N' values of the previous displacement step as per Eq. (3). This causes a slight inaccuracy, which can be minimised by using a very small displacement.

Eventually, either the out of balance force will reduce to zero, or reach a minimum and begin rising. If it reaches zero, then the mechanism is stable, and the values of c'_{mob} and Φ'_{mob} at this point are the

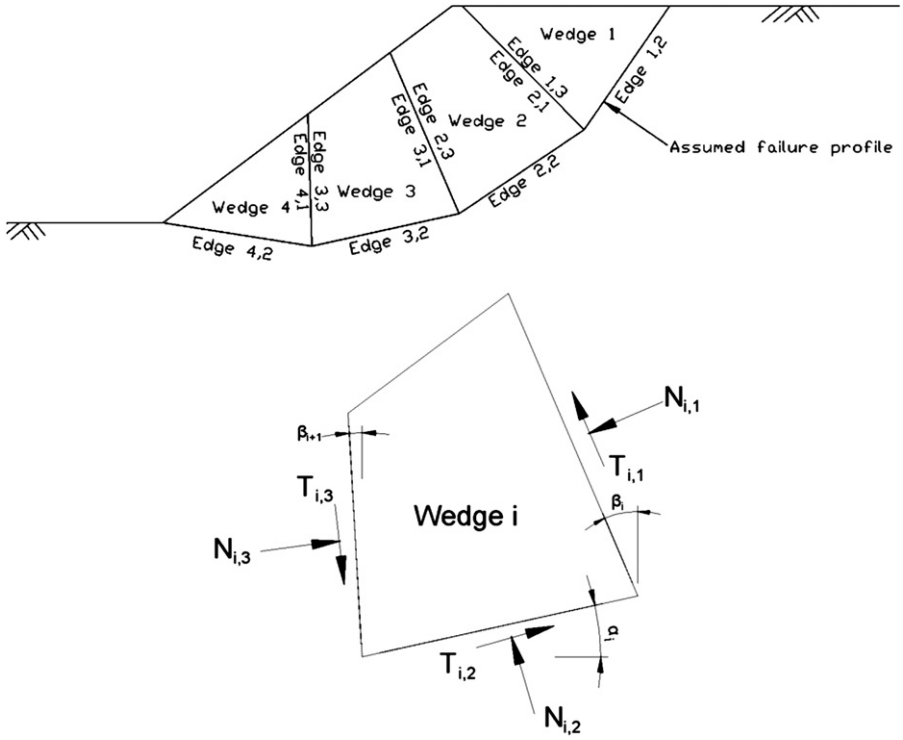

Fig. 3. Wedge boundaries of an arbitrary slip surface (also showing wedge boundary suffixes).

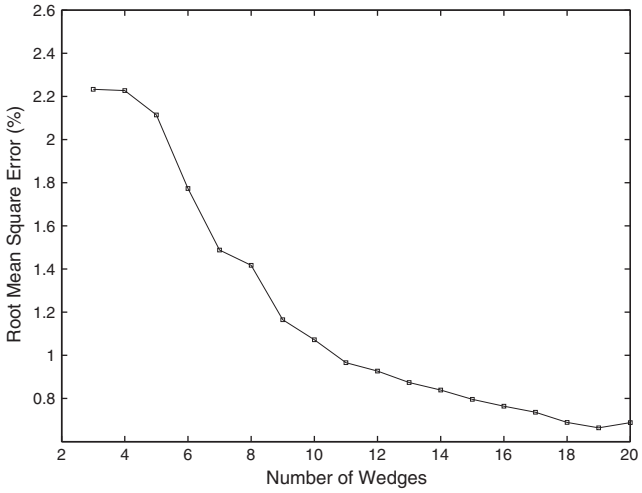

Fig. 4. Root mean square error of the model when predicting mobilised angle of shearing resistance (Φ'_{mob}) for a linear slip in a dry, non-cohesive soil.

equilibrium values. The particles at the base of all the different slip mechanisms store the highest values of c'_{mob} and Φ'_{mob}, and these are used to build the safety maps, as shown in the results (e.g. Fig. 9). If, however, the out of balance force does not reduce to zero, then the model domain cannot be in equilibrium, and the slip mechanism with the highest failure rate, i.e. the one with the fastest acceleration, will be modelled with the failure mechanics method, as detailed in Section 2.2.

The nature of this technique and the particle method means that it is convenient to represent multiple materials within the computational domain, and some failure surfaces may be such that equilibrium is not found until one material is failed and in residual strength, while the other is still approaching the peak value of Φ'_{mob}. Any material that ends up in residual strength can have its particle history stored, so that the model will not falsely attribute peak strength criteria to these particles.

2.2. Failure mechanics

Once the critical failure mechanism of the slope has been identified, the model uses a Smoothed Particle Hydrodynamics (SPH) type method to model the subsequent collapse of the bluff. The computational domain of the Bluff Morphology Model (BMM) applies scalar parameters to each of the particles, including mass, vertical earth pressure, pore water pressure, and velocity components. The values of these properties can be interpolated using the following equation, to compute any one of the scalar quantities $f(x)$ for any given particle:

$$f(x) = \sum_j f_j W\left(x - x_j\right) V_j \tag{7}$$

The scalar interpolation here of the function $f(x)$ is scaled by the function (f_j) of the particle j and V_j, being the volume of the particle. Volumes are explicitly calculated using the density and the mass, the latter of which remains constant for the duration of the simulation, ensuring conservation of mass. The smoothing function $W(x-x_j)$ is known as the kernel function, and although many types exist in SPH simulations, the cubic kernel was used for this model. This function acts as a weighted average for the summation of particles. This weighting is based on the proximity of the two particles, and although theoretically this should be applied to all particles irrespective of distance apart, the cubic kernel function is curtailed at a distance of $2h$, where h is a user defined parameter, but typically related to the initial particle spacing. This significantly reduces the computational time needed.

Similarly to the SPH method, the interacting particles are stored in a 'linked-list', which is updated with each time step, allowing more efficient programme runs.

Conservation of momentum and mass, as detailed by Monaghan (1994) is applied to the particle a in the form:

$$\frac{\partial v_a}{\partial t} = \sum_j m_j \left(\frac{p_a}{\rho_a^2} + \frac{p_j}{\rho_j^2} + \Pi_{aj} \right) \nabla_a W_{aj} + g \tag{8}$$

$$\frac{\partial \rho_a}{\partial t} = \sum_j m_j \left(v_a - v_j \right) \cdot \nabla_a W_{aj} \tag{9}$$

where j is all other particles within the radius of $2h$, p_j is the pressure; v_j the velocity; m_j the mass and ρ_j the density of the particle j. Π_{aj} is an empirical approximation of the viscosity effects (Monaghan, 1994), and W_{aj} is the kernel function. The SPH-type method used has been adapted from the open-source SPHysics code published on the University of Manchester website (SPHERIC, 2008). This code already includes the XSPH correction (Monaghan, 1989), and the tensile correction (Dyka and Ingel, 1995; Dyka et al., 1997; Monaghan, 2000) which has been integrated into the kernel function. This method uses a weakly compressible approach to fluid movement, and it has been adapted to study the flow of solids by including shear resistance and lateral earth pressure coefficients based on Rankine soil properties. Although negative pore water pressures can be modelled, negative soil pressures are rarely seen in large volumes within the field of interest, and typically act as a stabilising force, ergo these are considered negligible. The equations used to model the variable lateral earth pressures are shown below:

$$K_0 = 1 - \sin\left(\Phi'\right) \tag{10}$$

$$P_\theta = P_{vertical} * \left\{ K_a + \sin\left(\Phi'\right) * \cos(\theta) \right\} \tag{11}$$

where K_a is the Rankine earth pressure coefficient, for a soil with low lateral strain, and is dependant only on the maximum, not the mobilised Φ', and is related to the angular earth pressure as shown, where is the angle between the two particles and the vertical, and $P_{vertical}$ is the vertical pressure exerted by the bluff material weight above the particle.

The shear resistance of the bluff material is applied to particles within the smoothing length of $2h$, as are all the properties within the SPH method. This is computed using the SPH kernel, and is applied directly as a retardation of the particles, perpendicular to the vector between the two particles, such that:

$$\frac{\partial vs}{\partial t} = \sum_j \left(P_{\theta i} + P_{\theta j} \right) dx_c * \tan\left(\Phi'_r\right) * \sin(\theta) / (2 * pm_i) \tag{12}$$

where ∂vs is the change in the velocity of particle i caused by shear resistance. $P_{\theta i}$ is the pressure of particle i exerted in the direction of j, dx_c is the contact area between the two particles, which is calculated using the kernel function. pm_i is the mass of the model particle i, and Φ'_r is the residual shear resistance angle of the particles.

3. Results

3.1. Bluff slope stability analysis

A simple validation of the model involves testing linear slip surfaces in a dry non-cohesive soil. Using this method, the linear failure surfaces are tested and the Φ'_{mob} values needed for stability of the slip surface are computed. In order to satisfy the laws of motion, the theoretical mobilised angle of shearing resistance (Φ'_{mob}) will be equal to the inclination above the horizontal of the linear slip surface (α).

Fig. 4 shows the RMSE for the linear failure surfaces, depending on the number of wedges used, where the error is defined by the difference between the value of Φ'_{mob} and the inclination of the slip surface (α). As can be seen from Fig. 4, the accuracy increases dramatically with the increasing number of wedges until approaching a minimum value of 0.664%. However, the number of potential slip surfaces that the model can analyse decreases as the number of wedges increases. This is because each wedge must contain multiple particles for the method to work, and increasing wedge numbers, for any given model at a set particle count, decreases the number of particles per wedge. When considering a high number of wedges, the number of potential slip surfaces that contain sufficient particle numbers decreases, hence the number of analysed cases decreases. In order to find the critical slope and achieve a high accuracy at the same time, the optimum number of wedges has been found to be between five and twelve, depending on the scenario considered.

Consider a saturated ground, such that the pore water pressure is expressed by:

$$u = r_u * \gamma_{soil} * z \tag{13}$$

where u is the pore water pressure, γ_{soil} is the unit weight of the soil, r_u is the pore pressure coefficient, and z is the vertical depth below the free surface. Linear failure surfaces through a non-cohesive bluff material with an r_u value equal to the ratio of the unit weight of water to the unit weight of the material would be expected to mobilise an angle of shear resistance as shown below, where β_{slip} is the angle of inclination of the straight failure surface:

$$\tan\left(\Phi'_{mob}\right) = \tan\left(\beta_{slip}\right) / \left\{ 1 - \frac{r_u}{\cos^2\left(\beta_{slip}\right)} \right\}. \tag{14}$$

Fig. 5 shows the results of linear failure surface analysis when considering a saturated soil with pore pressure defined in Eq. (13). The saturated unit weight of the soil is 19.4, and therefore the ratio of the unit weights (r_u) is 0.5056. The observed relationship between the angle of a linear failure surface and that of Φ'_{mob} is linear, with a gradient very close to 2.0. It is apparent that there is some scatter in the results, with a tendency for slight over prediction of the value of Φ'_{mob} in the middle of the graph.

As the pore water pressure adds to the spatial variably of the model parameters, the error of this scenario is significantly larger than the previous benchmark case. However, this error decreases significantly with an increasing number of wedges. Fig. 6 shows the RMSE error compared to the number of wedges in the analysis, showing a minimum error of 1.4% for 11 wedges.

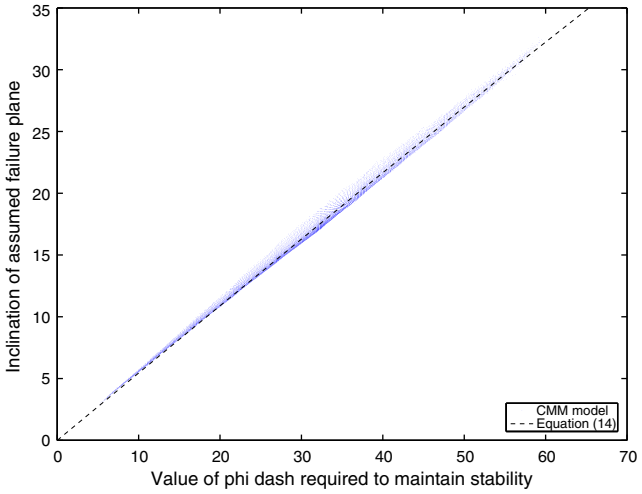

Fig. 5. Predicted mobilised angle of shearing resistance (Φ'_{mob}) for a linear slip in a wet, non-cohesive soil using 8 wedges.

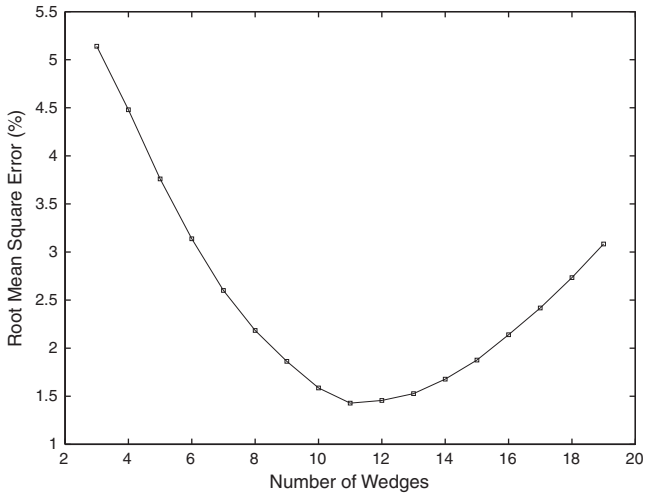

Fig. 6. Root mean square error of the model when predicting the mobilised angle of shearing resistance (Φ'_{mob}) for a linear slip in a wet, non-cohesive soil, where $\gamma_{soil}/\gamma_{water} = 1.91$.

Additional benchmark tests have been carried out to consider the ability of the programme to model circular, non-circular and compound slips in addition to linear translational slips. Due to the methodology used, the wedge boundaries are always linear, and as such a truly circular slip surface will be approximated into a polygonal form.

When considering a bluff material with no frictional strength, the cohesive strength needed for the stability of any given bluff geometry can be predicted by Taylor's Chart (Craig, 1974) which has been calculated using the principle of geometric similarity. The failure of a non-frictional, homogenous slope will always be a wide circular failure mechanism, extending as deep as possible into the bluff. For this reason, the solution is dependent on the depth to a firm stratum, and this is expressed as a factor of the slope height, *D*.

Fig. 7 shows a comparison of the Taylor's stability coefficient with the values predicted by the BMM. Each slope geometry is analysed by the BMM, and the most critical slip mechanism, i.e. the one that gives the lowest Factor of Safety (*FoS*), is outputted by the model, and subsequently used to give a stability coefficient N_s, as shown below:

$$N_s = \frac{C_u}{FoS * \gamma_{soil} * H} \tag{16}$$

where c_u is the maximum undrained shear strength, *FoS* is the Factor of Safety, and *H* is the height of the slope. This expected value of N_s also depends on the distance between the top of the slope and firm stratum (D^*H), where *H* is the slope height, and two cases have been considered, $D=1$ and $D=2$. The theoretical predictions converge rapidly after $D=2$, and as uniform undrained shear strength is extremely rare in practical applications with any real depth, greater values of *D* have been ignored.

Fig. 7 shows a good correlation between the theoretical and predicted values of N_s, although the values are slightly underpredicted for low slope angles, they are within reasonable tolerance and are more accurate when considering the steeper slope. As Taylor's stability coefficient is inversely proportional to the Factor of Safety, the under prediction implies that the *FoS* of the model was too high, probably caused by the critical slip mechanism not being found, which may in part be due to the linear approximation of the wedge boundaries. There is no real variation in the results when different densities or slope heights are computed. Changing the number of wedges decreases the error initially as a smoother slip profile is modelled, however increasing errors in adjusting the wedge boundaries to avoid overlap cause an increase in the error past 10 wedges, as seen in Fig. 8.

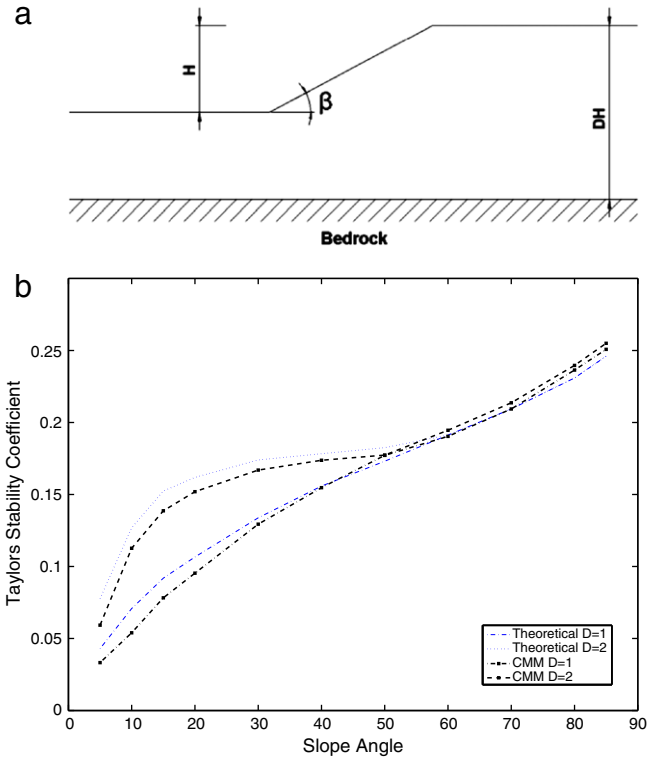

Fig. 7. Schematic of the slope domain (top). Taylor's stability coefficients for a non-frictional soil where the dash-dot lines show $D=1$ and the dotted lines $D=2$. The points are the computed slope values (bottom).

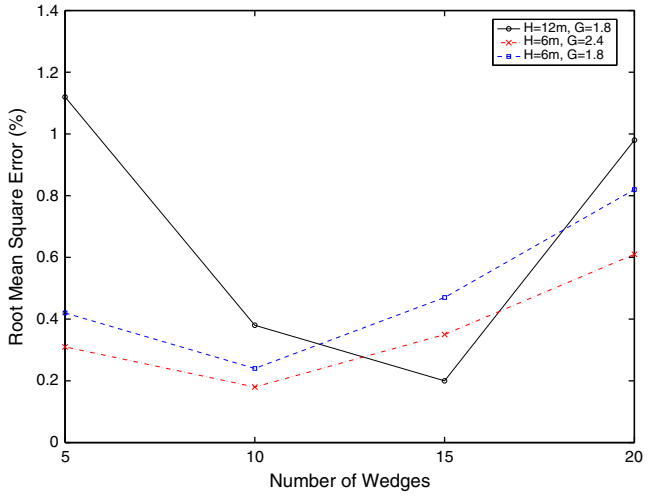

Fig. 8. Root mean square error of the model when predicting Taylor's stability coefficient for a non-frictional soil, for various numbers of wedges within each slip mechanism, where H is the cliff height in metres, and G is the density of the soil relative to the density of water.

Having considered the cases of zero frictional strength, and zero cohesive strength, a further case study is now considered with a homogenous clay type soil. The slope angle is 20°, with a height of 6 m. The soil considered has a cohesion intercept of 2.5 kN m^{-2}, and a peak friction angle of 20°. The water table is at the ground surface, and has an r_u value of 0.3.

The model tests slopes for all shapes from linear through arc and circular slips. The critical, i.e. the minimum value of Φ'_{mob} of each soil particle is recorded and as such an overall picture can be seen of the total of Φ'_{mob} at each particle within the slope. This allows

every particle to retain a *FoS*, and as such a detailed cross sectional profile is visible, as shown for another case, in Fig. 10.

Fig. 9 shows the validation of the geometry with a comparison to the analytical model of Slope/W (Durrani, 2007). The present BMM model allows for a highly detailed breakdown of the slope surface compared to the Slope/W data, but Fig. 9 shows an excellent agreement between the two data sets.

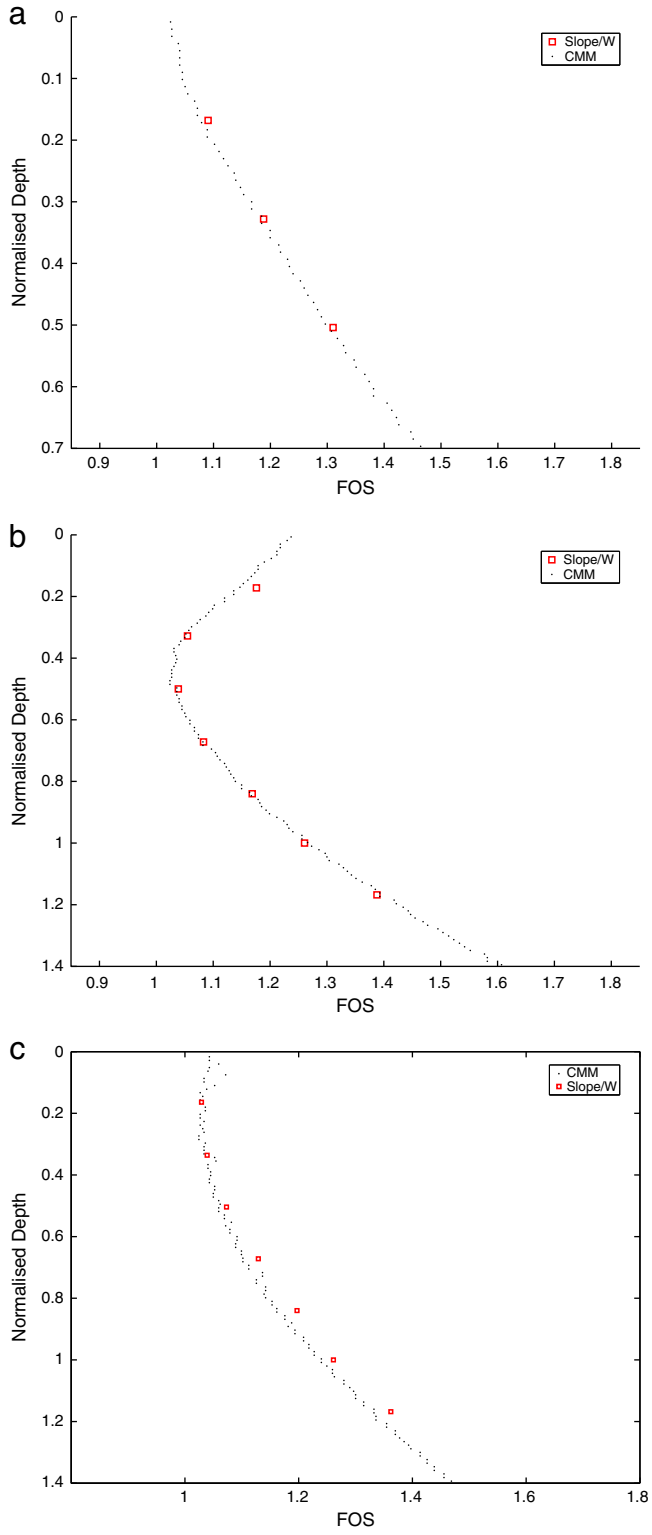

Fig. 9. Factor of Safety of a cohesive wet slope with the Cliff Morphology Model and the Slope/W (Finite Element Method) (Durrani, 2007). Analysis at the toe (a), midpoint (b) and crest (c) of the slope.

Due to the relationship between strain and strength mobilisation, it is possible to consider the strain of an essentially stable cliff surface, in addition to finding those that may be on the verge of a failure event. When considering a cliff constructed of a predominantly glacial deposit (Quinn et al., 2010), a stability analysis using generic soil properties for glacial till, the stability analysis for the entire slope can be seen in Fig. 10, suggesting a predominantly linear failure with a curvature towards the toe of the cliff. The slight anomalies in the form of the surface particles on the face of the cliff are due to the resolution of the model and should be discounted. It is likely that the stability of these particles is overrepresented. This stability map, agrees well with the description of failure (Quinn et al., 2010).

The lines in Fig. 10 show the surveyed cliff position, and indicate a similar mode and magnitude of failure to the model predictions. It is likely, as seen from the undulation between 5 and 10 m on the x-axis, that the failure in question was more complex than a single collapse. Indeed, although it is possible that tension cracks and toe erosion played a significant part in the failure of the slope, the new cliff surface still can be traced through the areas of significant instability, where the Factor of Safety is 1.45 or lower. This may well be an over-prediction of stability also due to the pore water, and rainfall around the time of the slip, which are not documented.

Having constructed the stability of the slope in question, it is easy to plot the lateral strain of the particles in this formation. Lateral strain over a measurable quantity can be converted into displacement, and Fig. 11 shows a comparison between the particle method of this paper, and the fast Lagrangian analysis of continuum (FLAC) code of Quinn et al. (2010). This method produces a plot of displacement and stress, not stability, however the concepts are related.

Fig. 11 shows a distribution of the lateral (x-direction) movement of the slope from Fig. 10, compared with retrospective analysis of the mass failure. This is based on the data presented by Quinn et al. (2010) in the Withernsea area of north-eastern England. The magnitude and distribution of the flow contours are similar, with a slightly more erratic distribution of the contours in the BMM, which is partially caused by the resolution clipping the boundaries on the base of the expected slip. An additional anomaly between the two results is the gradient at the top of the slip pattern. This is likely to be caused by tension cracking, or a significant weakness of the soil properties at the top of the slope that is not considered by the current BMM. However, the results show similarity in method and magnitude of failure mode, which is critical to the model's accuracy and applicability.

3.2. Bluff slope failures

Having considered the slope stability methods the model can also predict the significant collapse, failure movement and equilibrium position of the bluff, based on the critical slope mechanism. Once

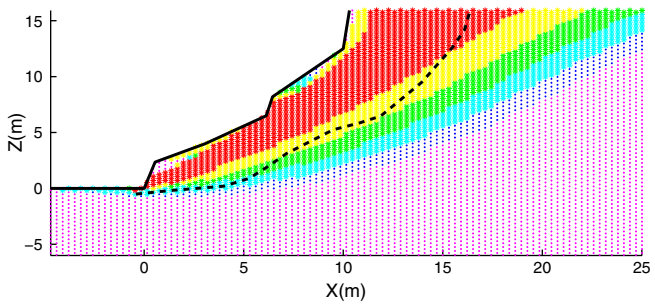

Fig. 10. Factor of Safety for a typical glacial till deposit cliff, showing surveyed positions of July 2007 (solid) and February 2008 (dashed) by Quinn et al. (2010).

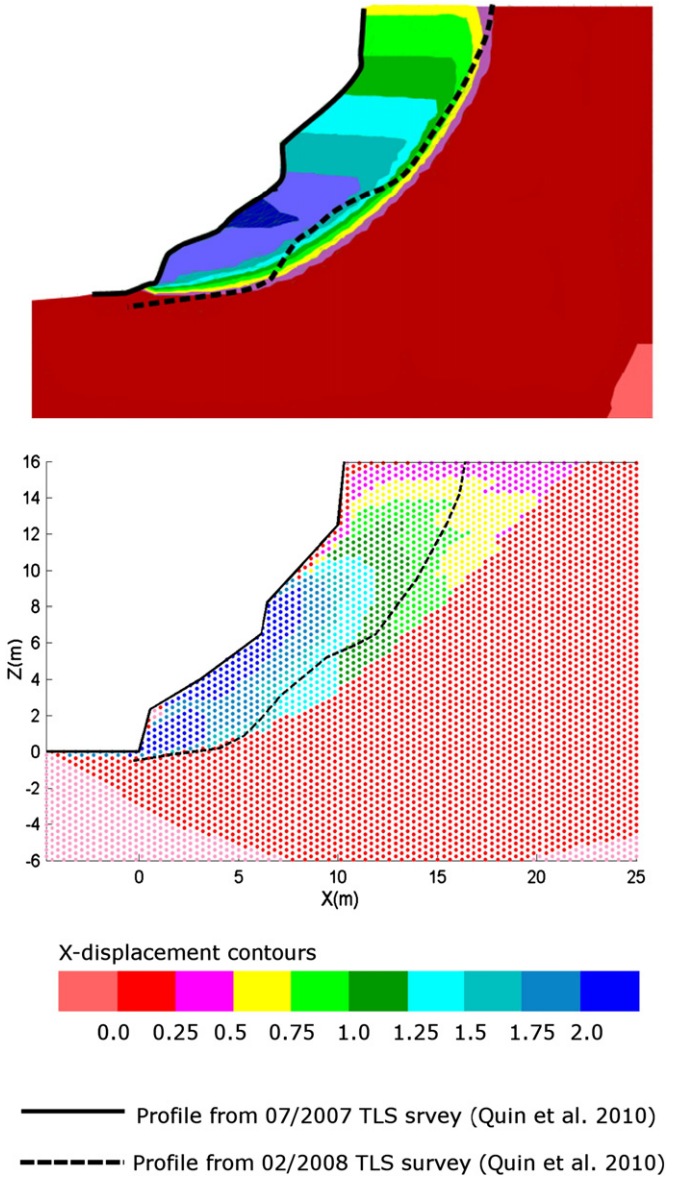

Fig. 11. Horizontal displacement of a glacial till failure. The preset Bluff Morphology Model (BMM) (above) compared to the Fast Lagrangian Analysis of continuum (FLAC) model (Quinn et al., 2010) (below).

the slope boundary enters the plastic deformation phase, the mobilised earth material collapses using the SPH adaption method previously outlined in Section 2.2.

When considering the collapsed profile of a bluff, the final equilibrium shape will depend on how catastrophic collapse is, i.e. the quantity of mobilised material, and the orientation of the failure plane, are critical parameters that control the final position of the collapsed material. This is likely to depend on the rate and magnitude of change of the bluff parameter that induces collapse. Bluff collapse can be induced by fluxes in pore water pressure, erosion, or reduction of material strength. The nature of the failure and change in the bluff profile will depend entirely on the volume of earth material mobilised, as shallow slips in a non-cohesive earth material will result in small scale "avalanching" as opposed to a deep seated rotational failure that will cause a catastrophic change to the final equilibrium profile of the bluff.

To induce a catastrophic bluff collapse and test the accuracy of the model, a sudden change of bluff parameters is used. In this case, a dambreak type scenario is examined, where a vertical bluff of non cohesive dry material is allowed to fall at $t=0$. The initial bluff geometry and parameters are identical to those used in the Distinct Element Method by Iwashita and Hakuno (1990). The initial geometry is a 3 m-high vertical slope, and the material is dry with a Φ'_{max} value of 11°, and a density of 2000 kg m^{-3}.

The Distinct Element Method by Iwashita and Hakuno (1990) is used as a comparison in Figs. 12 and 13, models the earth material as a mass-and-spring mechanism with non-uniform resolution, which can give rise to some unexpected behaviour when blocks of mass remain attached to their neighbours. This is especially noticeable in the overhang at 0.6 s in Fig. 11. The BMM model, by contrast, achieves a much smoother failure as a direct result of the kernel function, which is far closer to what is expected when considering such a large slip of a non-cohesive material. Whilst this smoother function is a more physical and expected result when considering non-cohesive material, the nature of the SPH collapse method in a highly cohesive material such as clay collapse remains an ongoing research question.

Fig. 12 clearly shows the collapse of a vertical bluff as a sudden mass movement, followed by some residual movement along the top of the failed earth material until equilibrium is reached. The two models predict similar initial failure patterns, with greater movement at the toe of the failed soil, creating an increasingly reclined front face, and smaller angle at the displaced bluff "edge". By 1.0 s, the front face of the bluff has become almost linear, and the methods diverge slightly as the BMM method shows the failed material bunching up at the leading edge, as opposed to the smooth linear residual plane of the Distinct Element Method by Iwashita and Hakuno (1990).

In Fig. 13 it can be clearly seen that both models predict the highest velocities at the surface of the slump, a phenomenon echoed by experimental results (Lube et al., 2005). The present BMM does not push the debris as far along the lower boundary level, which may in part be due to the separately applied boundary conditions of the Distinct Element Method by Iwashita and Hakuno (1990), as opposed to the method used by the authors, where the same properties of the earth material were used to define all boundary conditions.

4. Conclusions

A novel particle method of bluff morphology model has been constructed. It combines a multiple wedge displacement method with an adapted Weakly Compressible Smoothed Particle Hydrodynamics (WCSPH) method to compute the stability of the entire domain before modelling the failure and the subsequent equilibrium profile of a coastal bluff. The model shows good accuracy for predicting a wide range of stability scenarios and bluff material parameters. Model results of dry, non-cohesive earth material proved to be highly accurate, with root mean square errors of less than 2% for both dry and wet cases.

Tests on cohesive, non-frictional bluff materials have also been accomplished, with the relationship of Taylor's stability coefficients well predicted, especially at higher slope angles. In addition, the profile of the bluff is well predicted and compared well with an industry standard package, SLOPE/W. We also found that a more detailed cross-section profile can be achieved with high accuracy using the novel BMM model.

The lateral movement of a cliff can be extrapolated from the lateral strain produced in a typical cliff makeup. When compared to a surveyed cliff environment, the results show similarity in method and magnitude of failure mode, which is critical to the model's accuracy and applicability.

The particle method allows for accurate material tracking, and can model the collapse or failure of a bluff without complex mesh regeneration or straining. The equilibrium profile of the bluff failure is highly dependent on how unstable the pre-collapse conditions are, which is usually dependant on the rate of change of the destabilising parameter. Results have shown the ability of the model to simulate catastrophic failures under a sudden change of slope conditions with good accuracy.

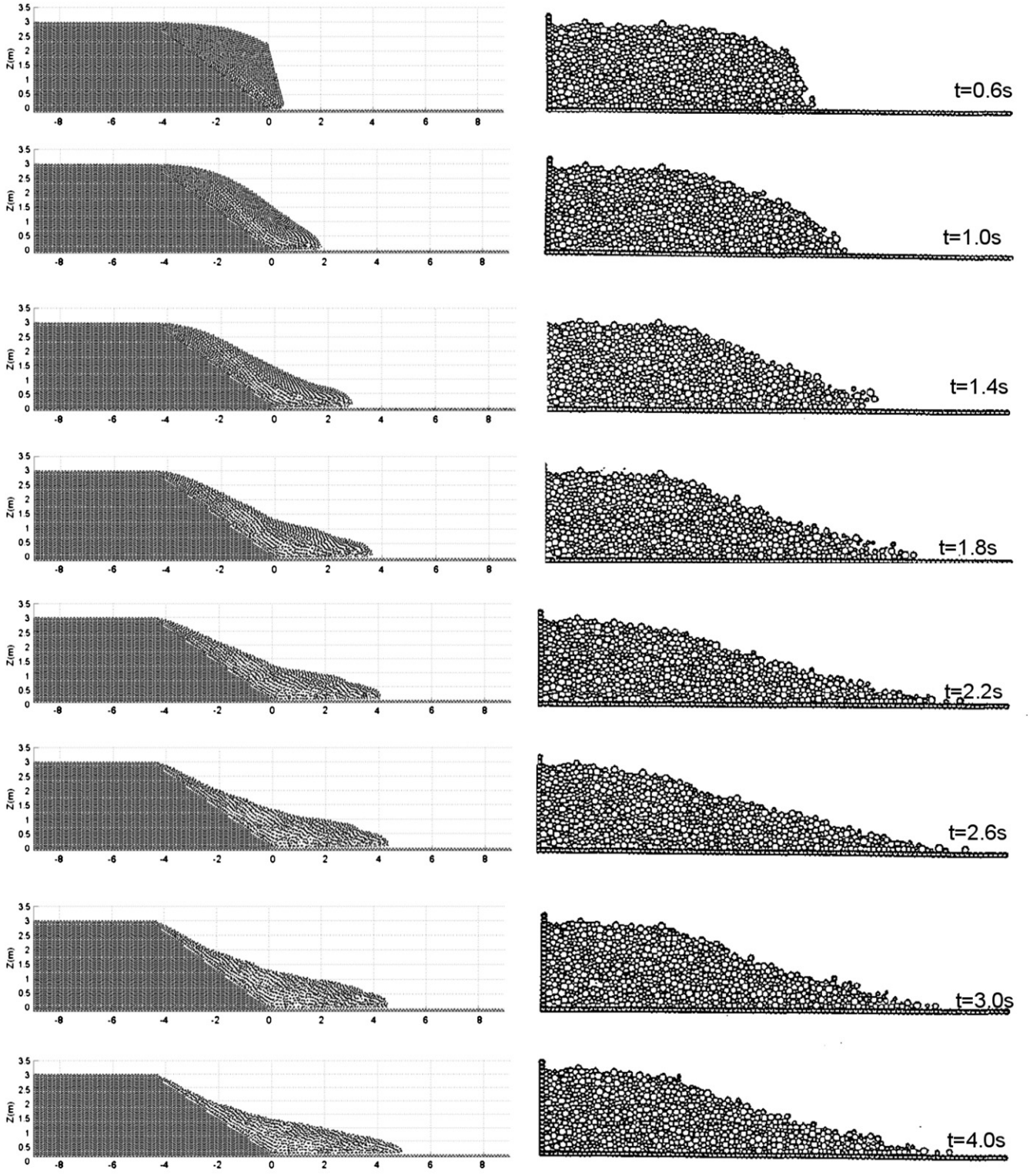

Fig. 12. Particle positions in a catastrophic collapse of a vertical cliff face. The present Bluff Morphology Model (BMM) (left) compared to Discrete Element Method (Iwashita and Hakuno, 1990) (right).

Sudden and catastrophic failures are very difficult to predict. Our model results indicate that although the final equilibrium position is relatively easier to correlate, the mechanism and movement of the mobilised material itself is highly variable. However, it is likely that a bluff section will fail first along a slip mechanism that has the highest "out-of-balance" force relative to the mobilised mass, i.e., the largest acceleration. In the case of multiple failure mechanisms existing in the bluff, which cannot reach equilibrium, the model used these parameters to identify the critical failure surface.

Overall, the new particle Bluff Morphology Model presented satisfies many of the conditions found in the modelling of coastal bluff collapse. At present the types of material modelled range from the

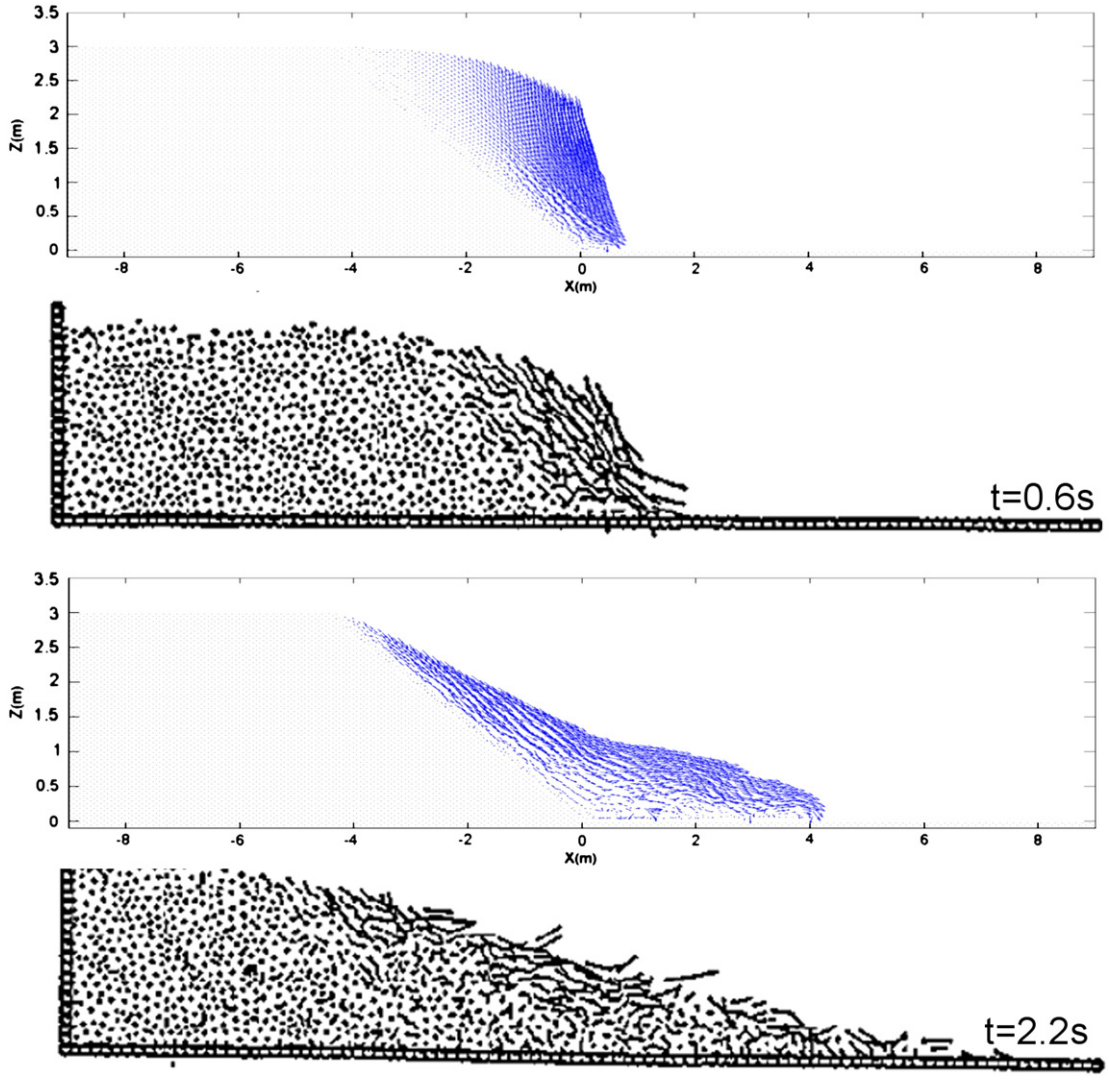

Fig. 13. Particle velocity vectors in a catastrophic collapse of a vertical cliff face. The present Cliff Morphology Model (BMM) (above) compared to Discrete Element Method (Iwashita and Hakuno, 1990) (below) at two different stages of failure.

purelycohesive to the purely frictional. The best model results can be achieved with a combination of these material parameters. The model is currently limited to bluffs with a fair percentage of homogeneity.

This model is capable of predicting the distribution of stability, and location and magnitude of failure mechanisms, and has the significant advantage of stability of a particle method. The model will be improved by including the variability of pore water pressures, two dimensional seepage and infiltration, and more considerable variation in the geotechnical and geological properties of the bluff material. These extensions are critical to extend the functionality of the model allowing for a greater breadth of real-world predictions, including the likelihood of collapse and collapse rates with sea level rise, as well as the changes in the Factor of Safety of a bluff with complex geology on the exposed face. The model presented offers a suitable platform with which to investigate episodic bluff collapse events themselves, and the detailed expositions from this model may serve to improve the accuracy and the forecasts of longer term models.

Acknowledgements

The authors would like to thank Professor Jim Griffiths for helpful discussions on coastal cliff geomorphology, and the authors would like to thank Dr. Alan Trenhaile and anonymous reviewers and editor for their comments that helped to improve the manuscript significantly.

References

Bromhead, E.N., Ibsen, M.L., 2004. Bedding-controlled coastal landslides in Southeast Britain between Axmouth and the Thames Estuary. Landslides 1, 131–141.
Caine, N., 1980. The rainfall intensity: duration control of shallow landslides and debris flows. Geografiska Annaler. Series A. Physical Geography 62, 23–27.
Chiu, T.Y., Dean, R.G., 1984. Methodology on coastal construction control line establishment. Tech. and Design Memorandum. Beaches and Shores Resource Center, Florida State University, Tallahessee, FL, pp. 84–86.
Chiu, T.Y., Dean, R.G., 1986. Additional comparisons between computed and measured erosion by hurricanes. Florida Department of Natural Resources, Beaches and Shores Technical and Design Memorandum, p. 17.
Craig, R.F. (Ed.), 1974. Soil Mechanics. Spon Press, London. 485 pp.
Dixon, N., Bromhead, E.N., 2002. Landsliding in London Clay coastal cliffs. Quarterly Journal of Engineering Geology & Hydrogeology 35, 327.
Donald, I.B., Chen, Z., 1997. Slope stability analysis by the upper bound approach: fundamentals and methods. Canadian Geotechnical Journal 34, 853–862.
Donald, I.B., Chen, Z., 1999. Modern wedge methods of slope analysis — their power and versatility. Second International Conference on Landslides, Slope Stability & the Safety of Infrastructures, pp. 13–24.
Durrani, I.K., 2007. Numerical modelling of discrete pile rows to stabilise slopes. PhD Thesis, Geomechanics, Civil Engineering, University of Nottingham.
Dyka, C.T., Ingel, R.P., 1995. An approach for tension instability in smoothed particle hydrodynamics (SPH). Computers and Structures 57, 573–580.
Dyka, C.T., Randles, P.W., Ingel, R.P., 1997. Stress points for tension instability in SPH. International Journal for Numerical Methods in engineering 40, 2325–2341.

Furlan, C., 2008. Hierarchical random effect models for coastal erosion of cliffs in the Holderness coast. Statistical Methods and Applications 17, 335–350.
Hutchinson, J.N., 1970. A coastal mudflow on the London Clay cliffs at Beltinge, North Kent. Geotechnique 20, 412–438.
Iverson, R.M., 2000. Landslide triggering by rain infiltration. Water Resources Research 36, 1897–1910.
Iwashita, K., Hakuno, M., 1990. Modified distinct element method simulation of dynamic cliff collapse. Structural Engineering/Earthquake Engineering, JSCE 7, 133–142.
Krahn, J., 2004. Stability Modeling with SLOPE/W. An Engineering Methodology, GEO-SLOPE/W. International Ltd, Canada. 408 pp.
Kriebel, D.L., 1986. Verification study of a dune erosion model. Shore and Beach 54, 8–15.
Kriebel, D.L., Dean, R.G., 1985. Numerical simulation of time-dependent beach and dune erosion. Coastal Engineering 9, 221–245.
Larson, M., Kraus, N.C., 1989. Report 1: Theory and Model Foundation. Report No. Coastal Engineering Research Center, U.S. Army Waterway Experiment Station, Vicksburg, MS.
Larson, M., Kraus, N.C., Byrnes, M.R., 1989. Report 2: Numerical Formulation and Model Tests. Report No. Coastal Engineering Research Center, U.S. Army Waterway Experiment Station, Vicksburg, MS.
Lee, E.M., Hall, J.W., Meadowcroft, I.C., 2001. Coastal cliff recession: the use of probabilistic prediction methods. Geomorphology 40, 253–269.
Lube, G., Huppert, H.E., Sparks, R.S.J., Freundt, A., 2005. Collapses of two-dimensional granular columns. Physical Review E 72, 41301.
Martins, F.B., Ferreira, P.M.V., Flores, J.A.A., Bressani, L.A., Bica, A.V.D., 2005. Interaction between geological and geotechnical investigations of a sandstone residual soil. Engineering Geology 78, 1–9.
McCall, R., 2008. The longshore dimension in dune overwash modelling. Development, verification and validation of XBeach. MscMsc Thesis, TU Delft, 280 pp.
McCombie, P.F., 2009. Displacement based multiple wedge slope analysis. Computers and Geotechnics 36, 332–341.
Monaghan, J.J., 1989. On the problem of penetration in particle methods. Journal of Computational Physics 82, 1–15.
Monaghan, J.J., 1994. Simulating free surface flows with SPH. Journal of Computational Physics 110, 399–406.
Monaghan, J.J., 2000. SPH without a tensile instability. Journal of Computational Physics 159, 290–311.
Quinn, J.D., Rosser, N.J., Murphy, W., Lawrence, J.A., 2010. Identifying the behavioural characteristics of clay cliffs using intensive monitoring and geotechnical numerical modelling. Geomorphology 120, 107–122.
Roelvink, D., Reniers, A., van Dongeren, A., van Thiel de Vries, J., McCall, R., Lescinski, J., 2009. Modelling storm impacts on beaches, dunes and barrier islands. Coastal Engineering 56, 1133–1152.
SPHERIC, 2008. SPHERIC Home Page. University of Manchester.
Trenhaile, A.S., 2009. Modeling the erosion of cohesive clay coasts. Coastal Engineering 56, 59–72.
Vandamme, J., Zou, Q., Reeve, D., Zou, S., 2009. Using a hybrid particle method to model coastal bluff collapse during extreme events. Coastal Dynamics Conference. World Scientific, Tokyo, Japan.
Walkden, M., Dickson, M., 2008. Equilibrium erosion of soft rock shored with a shallow or absent beach under increased sea level rise. Marine Geology 251, 75–84.
Walkden, M.J.A., Hall, J.W., 2005. A predictive mesoscale model of the erosion and profile development of soft rock shores. Coastal Engineering 52, 535–563.
Walstra, D.J., Roelvink, J.A., Groeneweg, J., 2000. 3D calculation of wave-driven cross-shore currents. Coastal Engineering Conference. ASCE American Society of Civil Engineers, pp. 1050–1063.
Zheng, J., Dean, R.G., 1997. Numerical models and intercomparisons of beach profile evolution. Coastal Engineering 30, 169–201.
Zou, S., 2007. Coastal Sediment transport simulation by smoothed particle hydrodynamics. PhD, Ph.D. thesis, Johns Hopkins University, Baltimore, Maryland, 157 pp.